Synthesis of ultrathin amorphous carbon films by plasma-stabilized direct-current filtered cathodic vacuum arc discharge

H.-S. Zhang and K. Komvopoulos

Department of Mechanical Engineering, University of California, Berkeley, California 94720

Abstract

Filtered cathodic vacuum arc (FCVA) deposition is characterized by plasma beam directionality and allows for independent substrate temperature control and substrate biasing. These important features make FCVA one of the leading techniques in plasma-source film deposition. However, although direct current (dc) arc discharge can greatly increase the deposition rate, arc instabilities in FCVA systems present major obstacles in maintaining the dc arc discharge. The present article presents a design that generates a "cusp" configuration of the magnetic field around the anode that stabilizes the dc arc discharge during film deposition. The efficiency of this design to maintain a stable dc discharge is demonstrated by amorphous carbon (*a*-C) films synthesized in the present FCVA system, using a three-dimensional (out-of-plane bending) magnetic filter to produce macroparticle-free ultrathin films. Raman, x-ray photoelectron spectroscopy (XPS), Rutherford backscattering spectroscopy (RBS), and nanoindentation results reveal that *a*-C films of relatively high hardness and tetrahedral carbon atom hybridization (sp^3) contents above 70 at% can be synthesized by applying pulsed bias to the substrate. Raman, XPS, RBS, and nanoindentation illustrate the efficacy of the plasma-stabilizing magnetic filter design to produce high-quality *a*-C films.

Submitted to *Review of Scientific Instruments*.

I. INTRODUCTION

Filtered cathodic vacuum arc (FCVA) is a low-temperature thin-film deposition technique that enables plasma beam manipulation.[1–5] However, plasma instabilities, macroparticle filtering difficulties, and low deposition efficiency are limiting factors. Despite significant evolution in the design of cathodic arc plasma filters[6–9] and arc discharge configurations,[3,10–13] tradeoffs between deposition rate, plasma stability, and plasma efficiency have yet to be resolved to fully utilize this deposition technique. Moreover, knowledge of plasma-generating mechanisms at different processing conditions is relatively sparse and semi-empirical. Although pulsed arc systems demonstrate high plasma efficiency, plasma can be maintained only for a fraction of the total deposition time, resulting in low film growth rates. In addition, pulsed arc systems require in-phase, duration-match control of arc pulsing and substrate bias pulsing. To increase the film growth rate and overcome difficulties in controlling the pulsing sequence, the FCVA system of the present study was equipped with a dc arc and the magnetic filter was designed to produce a "cusp configuration" of the magnetic field around the anode to enhance plasma stability and, in turn, enhance film growth rate.

The objective of this article is to present a dc arc plasma-stabilizing mechanism incorporated in a three-dimensional magnetic filter and demonstrate its effectiveness in the context of results obtained from amorphous carbon (*a*-C) films deposited on silicon with and without substrate biasing. The selection of *a*-C films for the comparative studies was motivated in light of their extensive use as protective overcoats in various applications[14–18] and well-characterized microstructures and mechanical properties. Results for the thickness, mass density, and carbon atom bonding of the deposited *a*-C films obtained with various microanalysis

techniques are presented to illustrate the effectiveness of the magnetic field plasma-stabilizing mechanism in producing high-quality *a*-C films.

II. FILTERED CATHODIC VACUUM ARC SYSTEM

Figure 1 shows schematics of the FCVA system. The plasma generated by an arc produced at the cathode between the cathode coil and the upstream coil is guided through the upstream, auxiliary, and downstream coils toward the substrate surface. For film uniformity, the 5-inch-diameter substrate holder is rotated during film deposition. Outside the downstream coil, four orthogonally mounted raster coils are used to raster the plasma beam (not shown in Fig. 1 for clarity). The temperature of the cathode and the substrate holder are controlled by water cooling. A base chamber pressure of less than 3×10^{-7} Torr is achieved by a cryopump. A 64-mm Kaufman ion source is used to sputter-clean the substrate surface by Ar^+ ion bombardment.

The magnetic field during dc arc discharging is shown in Fig. 2. The cathode consisting of any conductive solid material is mounted on a cylindrical shaft used to move the cathode relative to the tubular copper anode to maintain a fixed cathode-to-anode distance. A mechanical trigger strikes the cathode while it is biased at -50 V relative to the anode to ignite the plasma. The current due to the arc discharge is kept constant by a control circuit. Because the magnetic field generated by the cathode coil is opposite to that produced from the upstream coil, the magnetic field lines around the anode exhibit a "cusp" configuration that maintains the arc current at the cathode surface relatively to the cathode center and stabilizes the arc current by maintaining a continuous electron flow from the cathode to the anode. The current through the cathode coil can be varied up to a maximum value of 25.9 A. The dense wire winding (106–203 mm wiring diameter) of the cathode coil produces a strong magnetic field (2.17 mT/A at the cathode solenoid center) that enhances the ion current and improves the arc discharge.[11,19] Although this

magnetic field configuration stabilizes the plasma, most of the plasma is lost to the anode and only a small fraction travels parallel to the filter centerline toward the substrate. For a cathode consisting of pure carbon and a total arc discharge current of 70 A, the carbon ion flux rate at the substrate holder was measured to be ~1.48×10^{19} ions/m^2·s.

The magnetic fields of the upstream, auxiliary, and downstream coils are of the same direction and are continuous within the filter space. To enhance the filtering effect and guide the carbon plasma along the coil centerlines toward the substrate surface, the currents in the upstream, auxiliary, and downstream coils are usually set to their peak values (i.e., 30.5, 30.9, and 29.6 A, respectively) by a 233 mm-diameter wiring. The intensity of the magnetic field at the center of the upstream and downstream coils (normalized by the coil current) was measured to be 1.32 and 1.23 mT/A, respectively. The three-dimensional, out-of-plane bending configuration of these coils provides an effective means of depositing macroparticle-free thin films. Depending on the cathode material and the arc discharge current, the currents in the four raster coils must be adjusted to maintain the plasma at the substrate surface.

A pulsed bias voltage can be applied to the substrate holder by a dc voltage source and an electrical chopper (Spark-le V, Advanced Energy Industries). Both the pulse amplitude and the pulse frequency can be adjusted through the dc voltage source and the electrical chopper. A bias waveform of –100 V time-average value and 25 kHz frequency was recorded during carbon film deposition, as shown in Fig. 3.

III. DIRECT CURRENT ARC DISCHARGE AND PLASMA FORMATION

Electrons flow out of the cathode when an arc discharge is generated between the cathode and the anode. Pressure and electrical potential effects cause the arc current to be focused onto non-stationary tiny spots on the cathode surface, resulting in very high pressure gradients within

a distance of 1 mm from the cathode surface.[3,4] This leads to the expulsion of cathode material into plasma state of certain energy distribution and angle of flight. Plasma formation involves complex transitions of the cathode material from the solid phase to equilibrium, dense, liquid phases and, then, to nonequilibrium expanding plasma.[3,17] The magnetic field at the cathode surface where the plasma is first generated plays a very important role in stabilizing the arcing spots and orienting the plasma flow.[19] During film deposition in the current system, the superposition of the magnetic fields of the cathode coil (at its maximum current) and the upstream coil at the cathode surface produces a field intensity of 34.1 mT. The relatively high strength and cusp configuration of the magnetic field maintains the arc discharge current close the set level.

A three-dimensional filter is used to prevent macroparticle and/or droplet deposition onto the growing film surface. The strong magnetic field of the filter enhances the plasma and preserves its energy distribution. Because of the neutralizing effect, the ions travel close to the electrons guided by the magnetic field lines. Even though the net electrical charge in a given volume in the chamber is neutralized by the same spatial density of ions and electrons, the electrons move much faster than ions, resulting in much higher electron current.[9] For example, in the case of a 70 A arc discharge current produced from a graphite cathode, the electron and ion currents are equal to ~77 and ~7 A, respectively. Because the ion-to-electron current ratio affects sheath formation, high-frequency pulse biasing of the substrate is essential for preventing the build-up of a thick sheath due to excess electrons.[20]

In the absence of substrate biasing, ion bombardment of the growing film surface occurs with intrinsic ion energy distributions. The intrinsic ion energy in arc discharges has been measured for different elements.[4,19] The energy of the bombarding ions can be modulated by a

pulsed substrate bias that regulates the plasma sheath. Substrate pulsed biasing with a negative voltage causes the ions to accelerate through the plasma sheath, resulting in ion implantation into the film. Excess electrons are discharged during the off period of the pulse cycle when a zero or slightly positive voltage is applied to the substrate (Fig. 3). Pulsed biasing also prevents the expansion of the high-voltage plasma sheath leading to electrical breakdown and substrate arcing.[20,21] The ion energy at the substrate level can be determined from the bias waveform and the intrinsic ion energy distribution. High-energy ions can knock-off atoms from the film surface, resulting in resputtering of the deposited material. Since film growth depends on both densities of arriving ions and knocked-off film-forming atoms, substrate biasing decreases the film growth rate by increasing the resputtering yield.

IV. REPRESENTATIVE RESULTS FOR AMORPHOUS CARBON FILMS

The efficacy of the present FCVA system to produce high-quality thin films is demonstrated in this section in light of results revealing the microstructure and nanomechanical properties of amorphous carbon (*a*-C) films. A high-purity (99.999%) graphite cathode was used to deposit *a*-C films on 4-inch-diameter Si(100) substrates. For film uniformity, the silicon substrates were mounted on a substrate holder that was rotated at 60 rpm. Both the cathode and the substrate holder were cooled continuously during deposition by flowing water maintained at a temperature of ~10^{o}C. Prior to film deposition, the substrates were sputter-cleaned *in-situ* by an Ar^{+} beam of 500 eV energy, 16 mA current, and 60^{o} incident angle. The dc arc discharge current was set at 70 A. The voltage between the cathode and the anode during film deposition was 24 V. Earlier studies[2,10,16,21–23] have shown that the optimum ion energy for *a*-C film deposition is equal to ~120 eV, implying –100 V substrate bias voltage and ~20 eV original (intrinsic) ion energy. To demonstrate the significance of substrate biasing, two *a*-C films were deposited within 5 min

– one without substrate biasing (film A) and one with pulsed bias voltage of –100 V time-average value and 25 kHz frequency (film B). The film thickness was determined with a laser interferometer (NewView 100, ZYGO) having a 632.9-nm wavelength He-Ne laser beam by measuring the height of the step created by masking a portion of the substrate surface. The thickness of films A and B was found equal to 68 and 38 nm, respectively.

Figure 4 shows an X-ray diffraction (XRD) spectrum of film A obtained with a conventional X-ray beam of 0.15406 nm wavelength generated by a Cu-Kα X-ray tube (D500, Siemens), using 30 mA generator current, 40 kV generator voltage, 0.05^{o} step size, and 2 s step time. The absence of any significant crystalline reflections indicates that the synthesized carbon film is amorphous. The small peak at $2\theta = 38.8^{o}$ may be an indication of the existence of SiC nanocrystallites at the interface between the *a*-C film and the Si(100) substrate.[24] The formation of SiC may be attributed to C and Si atom interdiffusion across the interface during the film deposition due to the bombarding effect of energetic carbon ions.

Figure 5 shows Rutherford backscattering spectrometry (RBS) spectra for films A and B and bare Si(100) obtained with a custom-made RBS system that uses an energetic He^{+} ion beam generated from a 2.5 MeV Van de Graaff electrostatic accelerator. Backscattered ions were collected by two silicon detectors positioned at 165° with respect to the incident beam. The samples were tilted by 55^{o} from the incident beam direction. The density of C atoms per unit area can be determined by measuring the shift of the Si edge and/or the C peak area on top of the Si signal background. The two methods yielded very similar results, i.e., 9.9×10^{17} atoms/cm^2 for film A and 6.3×10^{17} atoms/cm^2 for film B. Using these results and the film thickness measurements, the density of films A and B was found to be 2.92 and 3.33 g/cm^3, respectively. Comparing these density values with those of graphite (~2.15 g/cm^3) and diamond (~3.51 g/cm^3),

it can be concluded that the sp^3 fraction in film B (–100 V bias) is much higher than that in film A (0 V bias). In fact, earlier studies[10,18,25,26] have shown that the sp^3 fraction in *a*-C films deposited under 0 and –100 V substrate bias voltage is approximately equal to 50 and 70 at%, respectively.

Figure 6 shows Raman spectra of films A and B obtained with the 488-nm line of an Ar^+ laser (model 85, Lexel) operated at 150 mW using a macroscopic optical setup. The refracted light was collected by a spectrometer (model 1877, SPEX) using an exposure time of 30 s in each scan. The spectra from two samples were aligned with the second Si signal peak at 991.2 cm^{-1}, as in a previous study.[2] After background subtraction, the Raman spectra shown in Fig. 6 were deconvoluted into two Gaussian peaks. The dominant peak (G band) at 1589.8 and 1584.8 cm^{-1} in the spectra of films A and B, respectively, corresponds to the in-plane Raman mode of graphite.[27,28] The small peak (D band) at 1372.2 and 1349.2 cm^{-1} in the spectra of films A and B, respectively, is attributed to small graphitic domains.[22,27] The D-to-G band area ratio, is equal to 0.246 and 0.207 for films A and B, respectively, suggesting relatively high sp^3 content.[22,28] Since Raman is sensitive to the sp^2 hybridization and largely insensitive to the sp^3 hybridization,[22,27,28] the lower intensity of the Raman spectrum of film B compared to that of film A is attributed to the higher sp^3 content of film B, consistent with the RBS results.

Figure 7 shows X-ray photoelectron spectroscopy (XPS) C1s spectra for films A and B obtained with a monochromatic X-ray source of Al-Kα (1486.6 eV) of a spectrometer (Kratos Analytical) operated at pass energy of 35.75 eV. The C1s spectra were acquired in 50-ms steps of energy equal to 0.05 eV and were deconvoluted after performing Shirley inelastic background subtraction.[29] A detailed description of the deconvolution method can be found elsewhere.[30] Six Gaussian distributions of characteristic binding energies associated with certain carbon chemical

states were fitted to each C1s envelope. The C1s-1, C1s-2, and C1s-3 distributions correspond to sp^1, sp^2, and sp^3carbon atom hybridizations, respectively. The sp^3 carbon fractions in the amorphous phases of films A and B, estimated from the deconvolution of the C1s XPS spectra using the method proposed by Jackson and Nuzzo[31] and Diaz et al.,[32] was found equal to >50 and >70 at%, respectively. The C1s-4, C1s-5, and C1s-6 distributions are attributed to bonding of C atoms with O atoms from the ambient chemisorbed at the film surface.[30,33]

Figure 8 shows representative nanoindentation curves of films A and B obtained with a surface force microscope[34] consisting of an atomic force microscope (Nanoscope II, Digital Instruments) retrofitted with a capacitive force transducer (Triboscope, Hysitron) equipped with a conospherical diamond tip of nominal radius of curvature equal to ~67 nm calibrated with an ultrasmooth fused quartz sample of in-plane modulus $E/(1-\nu^2) = 69.6$ GPa, where E is the elastic modulus and ν is the Poisson ratio. The small hysteresis area between the loading and unloading curves of the nanoindentation responses, corresponding to dissipation energies of ~0.127 pJ (film A) and ~0.135 pJ (film B) and negligibly small residual indentation depths (~88% elastic recovery for each film) indicate that indentation depths >20% of the thickness of these *a*-C films (or maximum indentation load of 150 μN) resulted in predominantly elastic deformation.

Figure 9 shows the mean contact pressure and in-plane elastic modulus of films A and B versus the maximum tip displacement for a triangular loading function with loading and unloading times both equal to 2 s. The mean contact pressure was calculated as the ratio of the maximum load to the projected contact area of the diamond tip and the in-plane modulus from the stiffness estimated at the maximum displacement point of the unloading curve.[24,34] Due to the substrate effect, both measurements give the "effective" mean pressure and in-plane modulus of the *a*-C film/Si(100) substrate medium. The initial increase of the mean pressure with the

maximum displacement is due to the evolution of subsurface plasticity. The maximum mean pressure reached at a displacement of ~20 nm for both films corresponds to the effective hardness of the film-substrate medium.[34,35] For films A and B, the effective hardness is equal to ~80 and ~55 GPa, respectively. Despite the higher sp^3 content of film B, the effective hardness is less than that of film A because of the more significant substrate effect on the contact pressure resulting from the higher displacement-to-thickness ratio at the peak contact pressure for film B than film A. The in-plane modulus of both media decreases with the increase of the indentation depth, tending to approach that of the substrate. Similar to the effective hardness, the substrate effect on the effective in-plane modulus is more pronounced for the thinner film B. Considering the in-plane modulus (150 GPa) and hardness (~8 GPa) of the Si(100) substrate, the results shown in Fig. 9 demonstrate a significant enhancement of both surface elastic stiffness and penetration resistance by the thin *a*-C films.

V. SUMMARY

The design of a special magnetic field for stabilizing the plasma generated by a dc FCVA discharge in a three-dimensional magnetic filter was presented and its capacity to produce high-quality thin films was demonstrated by synthesizing *a*-C films under unbiased and optimum bias deposition conditions. The "cusp configuration" of the magnetic field, generated by the opposite directions of the cathode coil and the upstream coil, produced a stable dc arc discharge that enabled fast deposition of dense films. XRD, RBS, Raman, and XPS analyses yielded insight into the bonding structure of *a*-C films produced by the dc arc discharge of the magnetic-field plasma-stabilizing mechanism. The high sp^3 content (>50% without bias and >70% with pulsed bias), high density (3.33 g/cm^3 with bias and 2.92 g/cm^3 without bias), and significantly

improved surface nanomechanical properties by the deposited *a*-C films demonstrated the effectiveness of the stable plasma produced in the present FCVA system.

ACKNOWLEDGMENTS

This work was supported by the Computer Mechanics Laboratory at the University of California at Berkeley. The authors are grateful to A. Anders and J. W. Ager III for helpful discussions, I. Sharp for Raman analysis, and K. M. Yu for assistance in obtaining the RBS spectra.

REFERENCES

[1]A. Anders, IEEE Trans. Plasma Sci. **29**, 393 (2001).

[2]S. Anders, A. Anders, I. G. Brown, B. Wei, K. Komvopoulos, J. W. Ager III, and K. M. Yu, Surf. Coat. Technol. **68-69**, 388 (1994).

[3]A. Anders, Surf. Coat. Technol. **93**, 158 (1997).

[4]E. Byon and A. Anders, J. Appl. Phys. **93**, 1899 (2003).

[5]A. Anders, IEEE Trans. Plasma Sci. **30**, 108 (2002).

[6]A. Anders, Surf. Coat. Technol. **120-121**, 319 (1999).

[7]A. Anders and R. A. MacGill, Surf. Coat. Technol. **133-134**, 96 (2000).

[8]G. F. You, B. K. Tay, S. P. Lau, D. H. C Chua, and W. I. Milne, Surf. Coat. Technol. **150**, 50 (2002).

[9]T. Schűlke and A. Anders, IEEE Trans. Plasma Sci. **25**, 660 (1997).

[10]V. S. Veerasamy, G. A. J. Amaratunga, W. I. Milne, J. Robertson, and P. J. Fallon, J. Non-Crys. Solids **164-166,** 1111 (1993).

[11]B. F. Coll, P. Sathrum, R. Aharonov, and M. A. Tamor, Thin Solid Films **209**, 165 (1992).

[12]B. Schultrich, H.-J. Scheibe, D. Drescher and H. Ziegele, Surf. Coat. Technol. **98**, 1097 (1998).

[13]T. Schuelke, T. Witke, H.-J. Scheibe, P. Siemroth, B. Schultrich, O. Zimmer and J. Vetter, Surf. Coat. Technol. **120-121**, 226 (1999).

[14]T. Yamamoto and H. Hyodo, Tribol. Inter. **36**, 483 (2003).

[15]B. Petereit, P. Siemroth, H.-H. Schneider, and H. Hilgers, Surf. Coat. Technol. **174-175**, 648 (2003).

[16]J. Robertson, Thin Solid Films **383**, 81 (2001).

[17]B. Bhushan, Diamond Relat. Mater. **8**, 1985 (1999).

[18]H. Han, F. Ryan, and M. McClure, Surf. Coat. Technol. **120-121**, 579 (1999).

[19]A. Anders and G. Y. Yushkov, J. Appl. Phys. **91**, 4824 (2002).

[20]A. Anders, Surf. Coat. Technol. **183**, 301 (2004).

[21]G. M. Pharr, D. L. Callahan, S. D. McAdams, T. Y. Tsui, S. Anders, A. Anders, J. W. Ager III, I. G. Brown, C. S. Bhatia, S. R. P. Silva, and J. Robertson, Appl. Phys. Lett. **68**, 779 (1996).

[22]B. K. Tay, X. Shi, H. S. Tan, H. S. Yang, and Z. Sun, Surf. Coat. Technol. **105,** 155 (1998).

[23]T. A. Friedmann, J. P. Sullivan, J. A. Knapp, D. R. Tallant, D. M. Follstaedt, D. L. Medlin, and P. B. Mirkarimi, Appl. Phys. Lett. **71**, 3820 (1997).

[24]W. Lu, K. Komvopoulos, P. Patsalas, C. Charitidis, M. Gioti, and S. Logothetidis, Surf. Coat. Technol. **168**, 12 (2003).

[25]Z. Feng, S. Anders, A. Anders, J. W. Ager III, I. G. Brown, K. Komvopoulos, and D. B. Bogy, Diamond Relat. Mater. **5**, 1080 (1996).

[26]A. C. Ferrari, A. Libassi, B. K. Tanner, V. Stolojan, J. Yuan, L. M. Brown, S. E. Rodil, B. Kleinsorge, and J. Robertson, Phys. Rev. B **62,** 11089 (2000).

[27]M. Yoshikawa, G. Katagiri, H. Ishida, A. Ishitani, and T. Akamatsu, J. Appl. Phys. **64**, 6464 (1988).

[28]M. A. Tamor and W. C. Vassell, J. Appl. Phys. **76,** 3823 (1994).

[29]D. A. Shirley, Phys. Rev. B **5**, 4709 (1972).

[30]D. Wan and K. Komvopoulos, J. Phys. Chem. C **111**, 9891 (2007).

[31]S. T. Jackson and R. G. Nuzzo, Appl. Surf. Sci. **90**, 195 (1995).

[32]J. Diaz, G. Paolicelli, S. Ferrer, and F. Comin, Phys. Rev. B **54**, 8064 (1996).

[33]W. Lu, K. Komvopoulos, and S. W. Yeh, J. Appl. Phys. **89**, 2422 (2001).

[34]W. Lu and K. Komvopoulos, J. Tribol. **123**, 641 (2001).

[35]L. Kogut and K. Komvopoulos, J. Mater. Res. **19**, 3641 (2004).

List of Figures

FIG. 8. Nanoindentation curves of *a*-C films synthesized under (a) zero bias (film A) and (b) –100 V, 25 kHz bias (film B) for maximum load of 150 μN and loading/unloading times equal to 2 s.

FIG. 9. Effective mean contact pressure and in-plane modulus for *a*-C films synthesized under (a) zero bias (film A) and (b) –100 V, 25 kHz bias (film B).

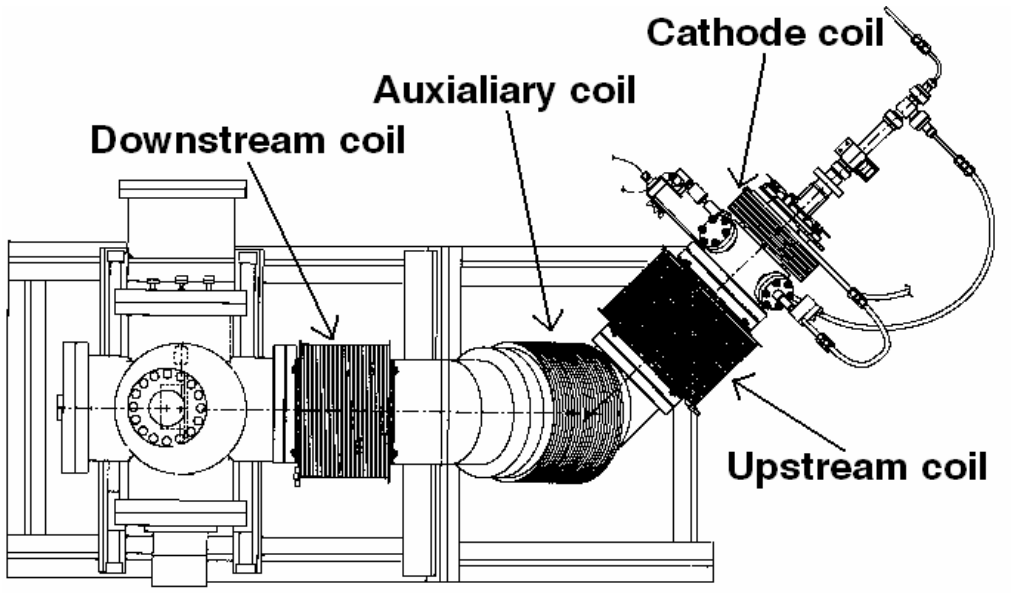
Cathode coil
Auxialiary coil
Downstream coil
Upstream coil

(a)

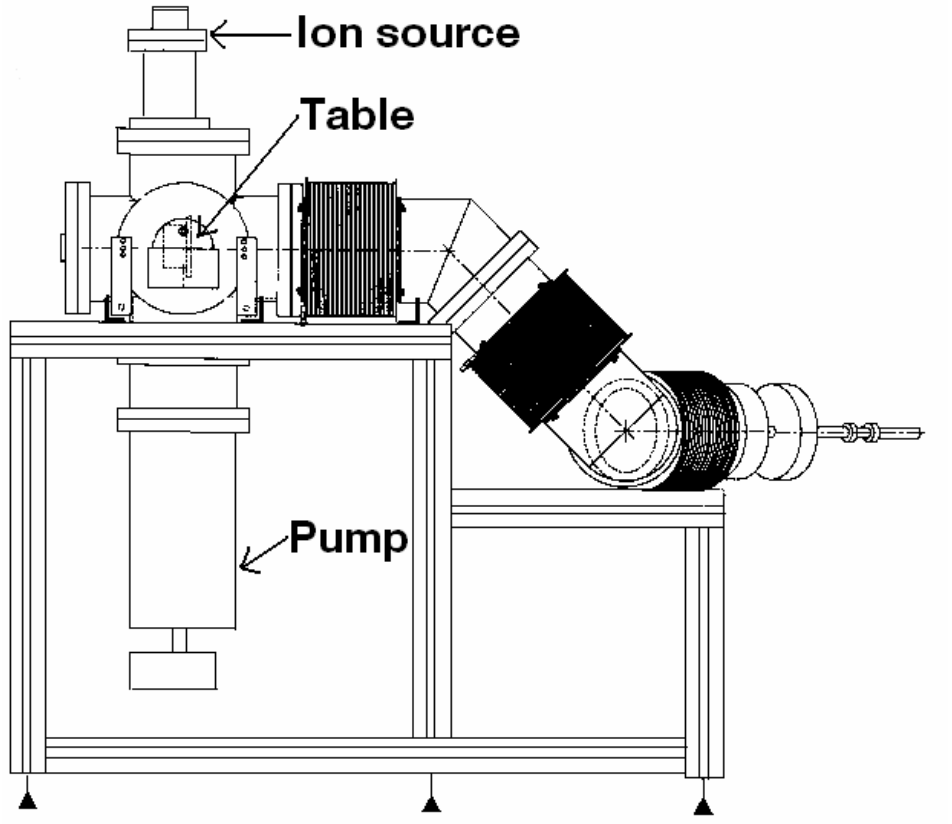
Ion source
Table
Pump

(b)

Figure 1

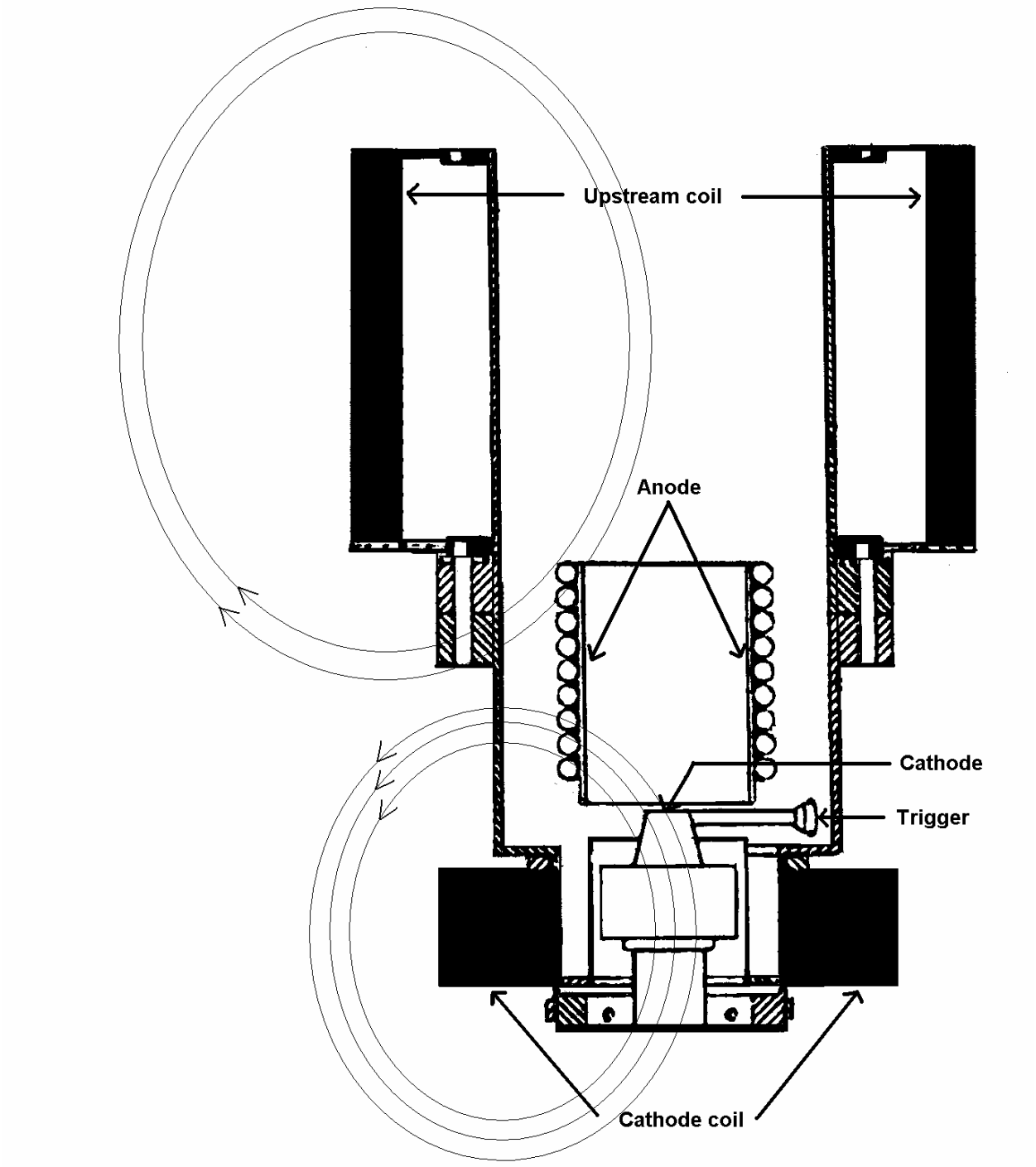

Figure 2

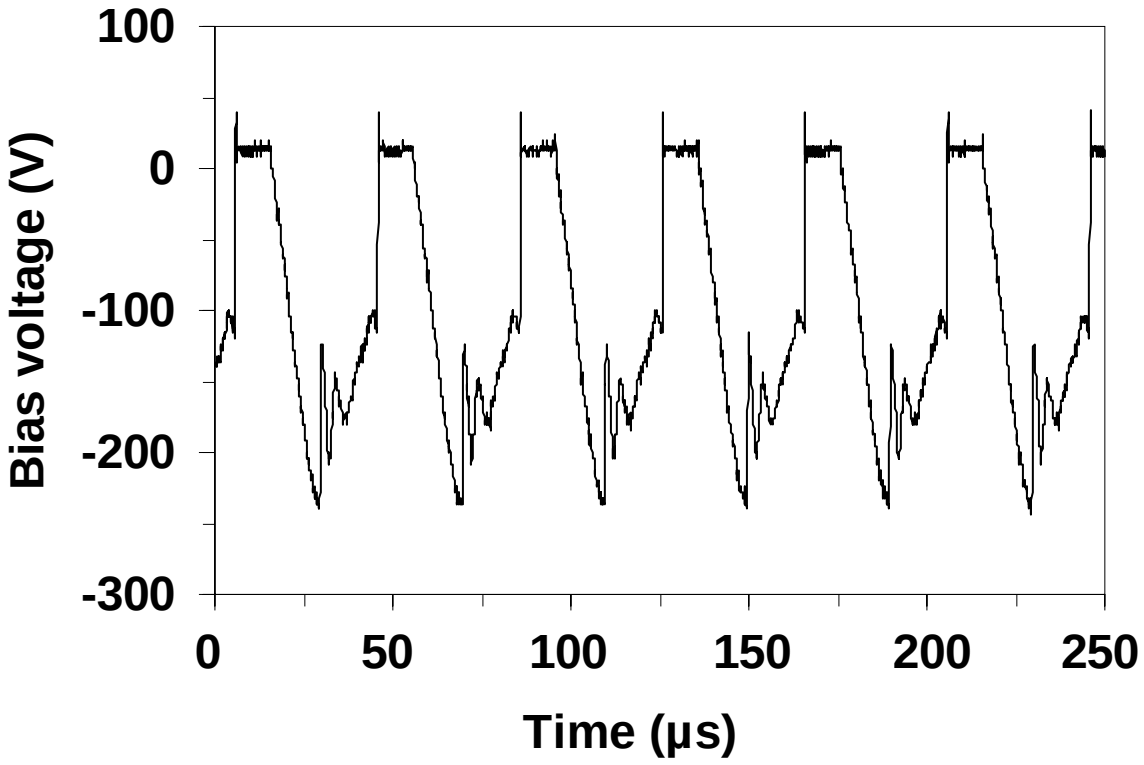

Figure 3

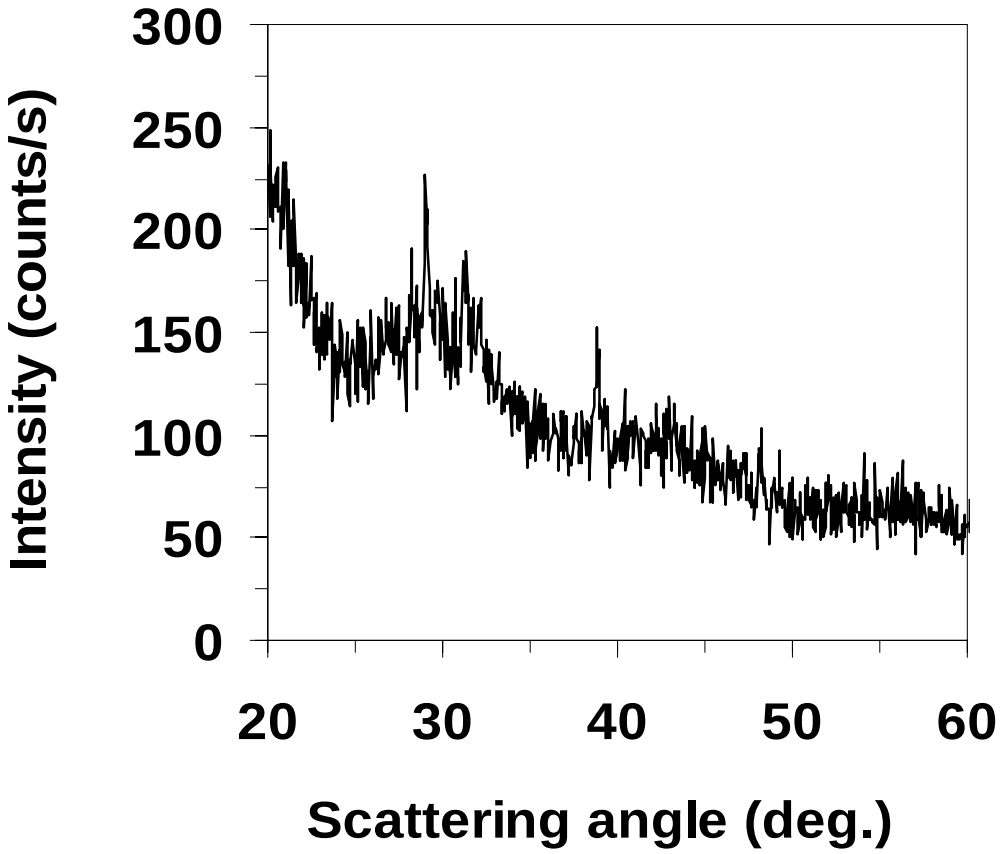
300
250
200
150
100
50
0
Intensity (counts/s)
20
30
40
50
60
Scattering angle (deg.)

Figure 4

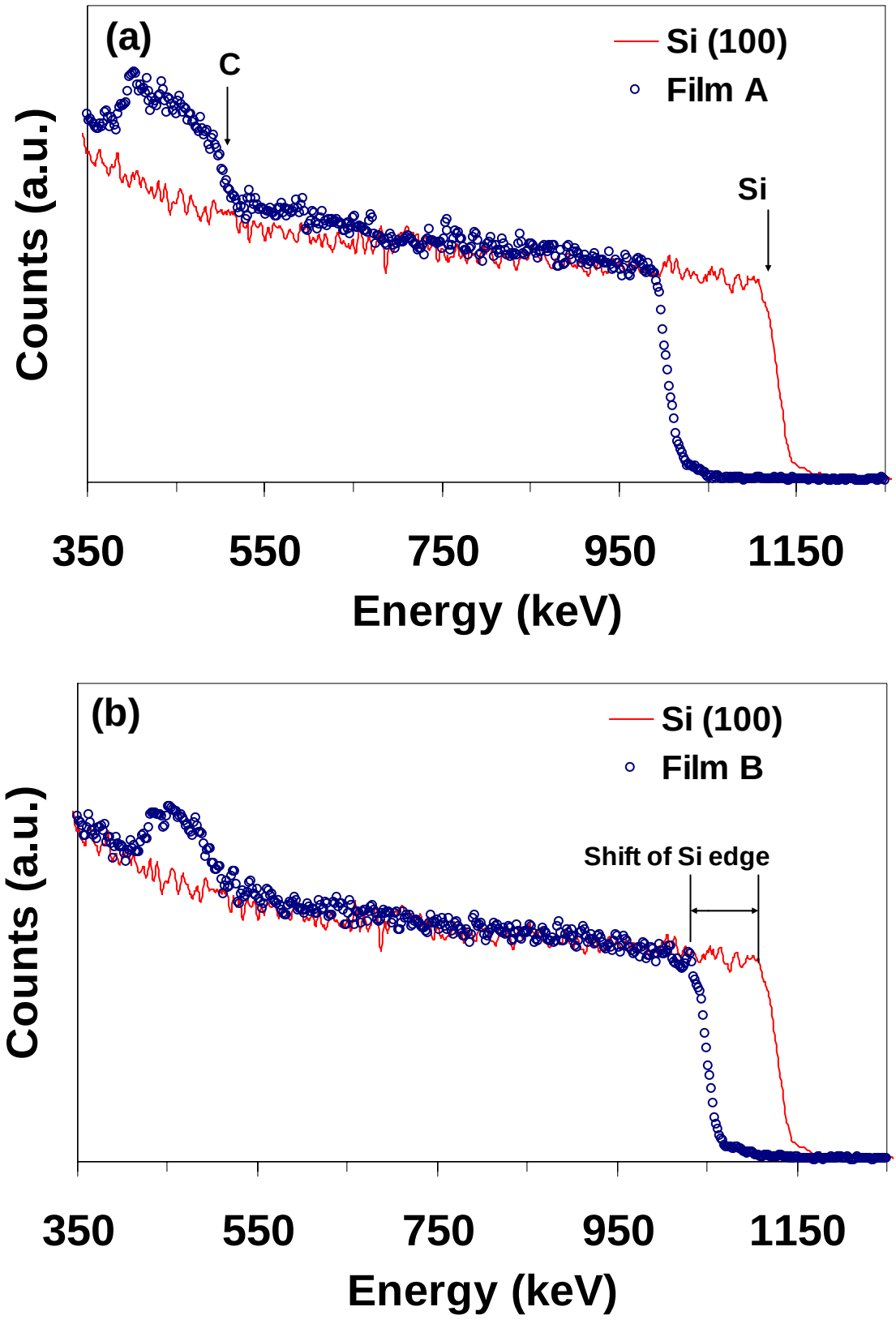
(a)
C
Si
Si (100)
Film A
Counts (a.u.)
350
550
750
950
1150
Energy (keV)
(b)
Si (100)
Film B
Shift of Si edge
Counts (a.u.)
350
550
750
950
1150
Energy (keV)

Figure 5

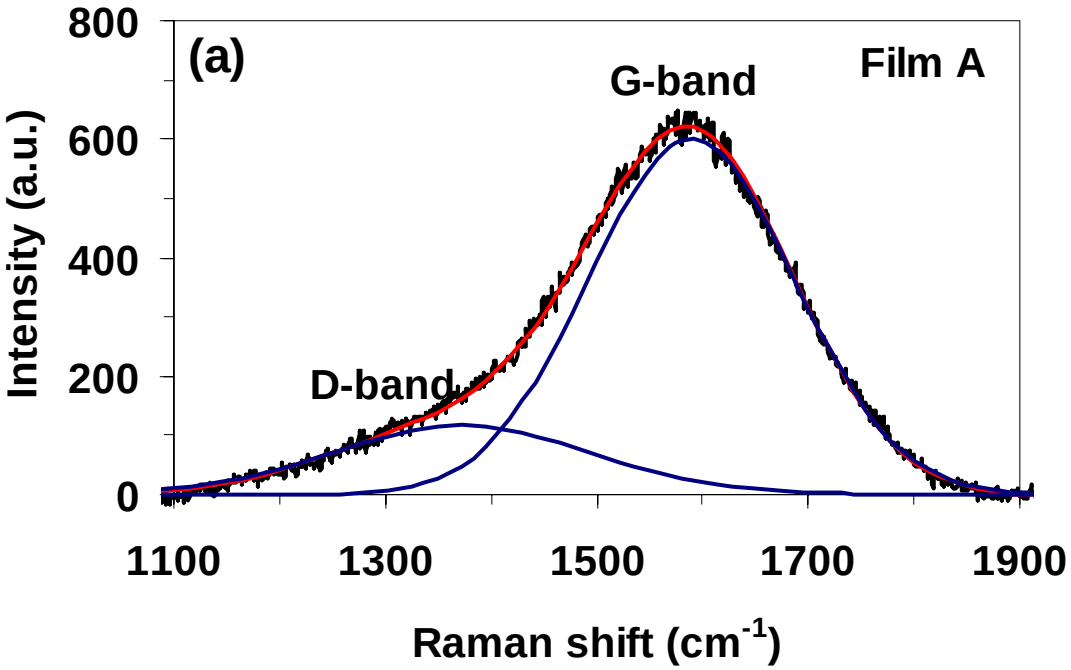
(a)
Film A
G-band
D-band
Intensity (a.u.)
800
600
400
200
0
1100
1300
1500
1700
1900
Raman shift (cm-1)

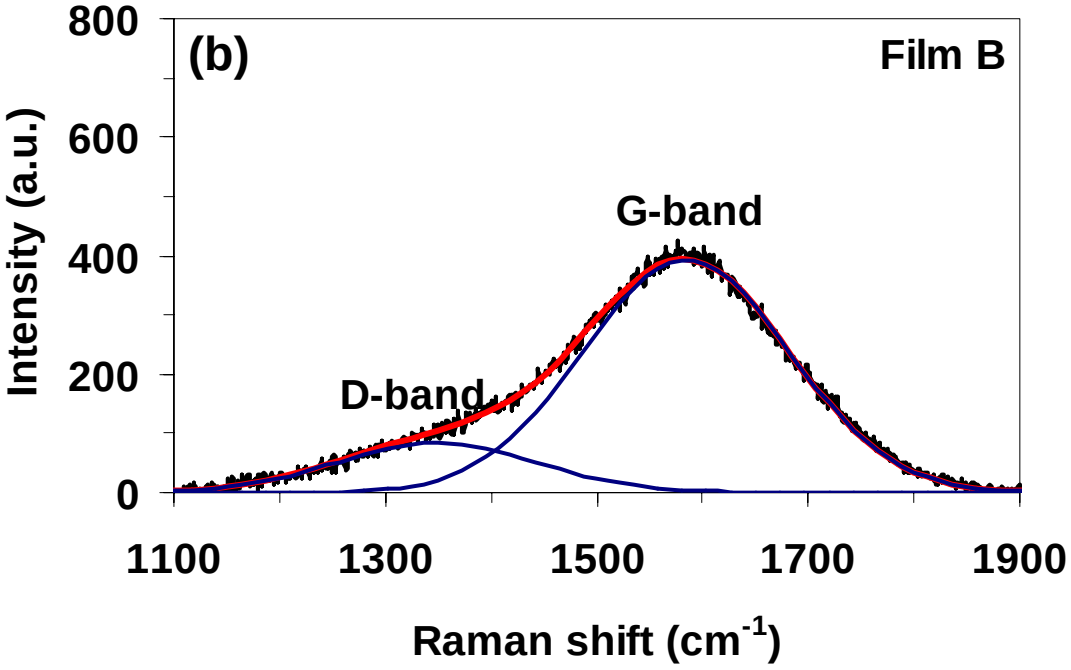
(b)
Film B
G-band
D-band
Intensity (a.u.)
800
600
400
200
0
1100
1300
1500
1700
1900
Raman shift (cm-1)

Figure 6

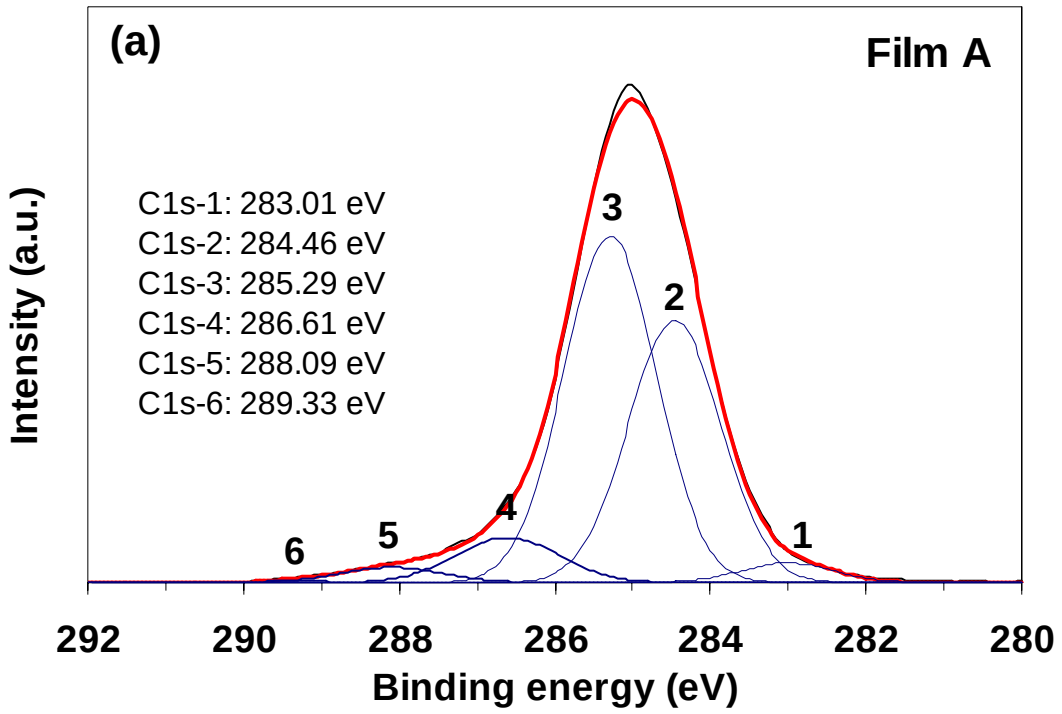
(a)
Film A
C1s-1: 283.01 eV
C1s-2: 284.46 eV
C1s-3: 285.29 eV
C1s-4: 286.61 eV
C1s-5: 288.09 eV
C1s-6: 289.33 eV
Intensity (a.u.)
292
290
288
286
284
282
280
Binding energy (eV)

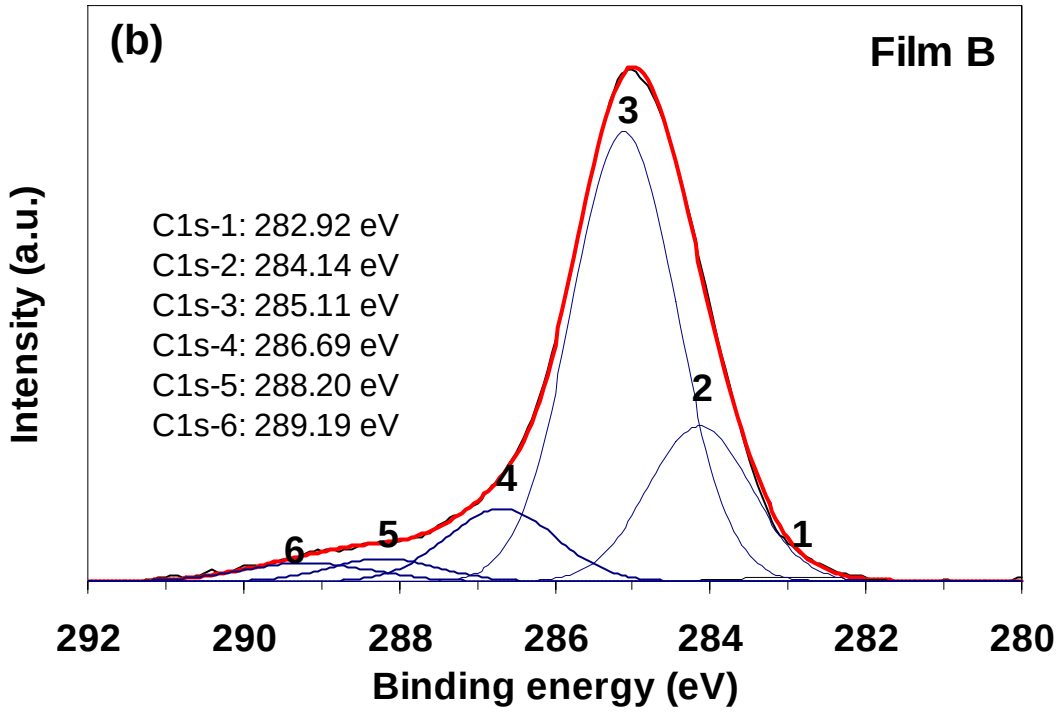
(b)
Film B
C1s-1: 282.92 eV
C1s-2: 284.14 eV
C1s-3: 285.11 eV
C1s-4: 286.69 eV
C1s-5: 288.20 eV
C1s-6: 289.19 eV
Intensity (a.u.)
292
290
288
286
284
282
280
Binding energy (eV)

Figure 7

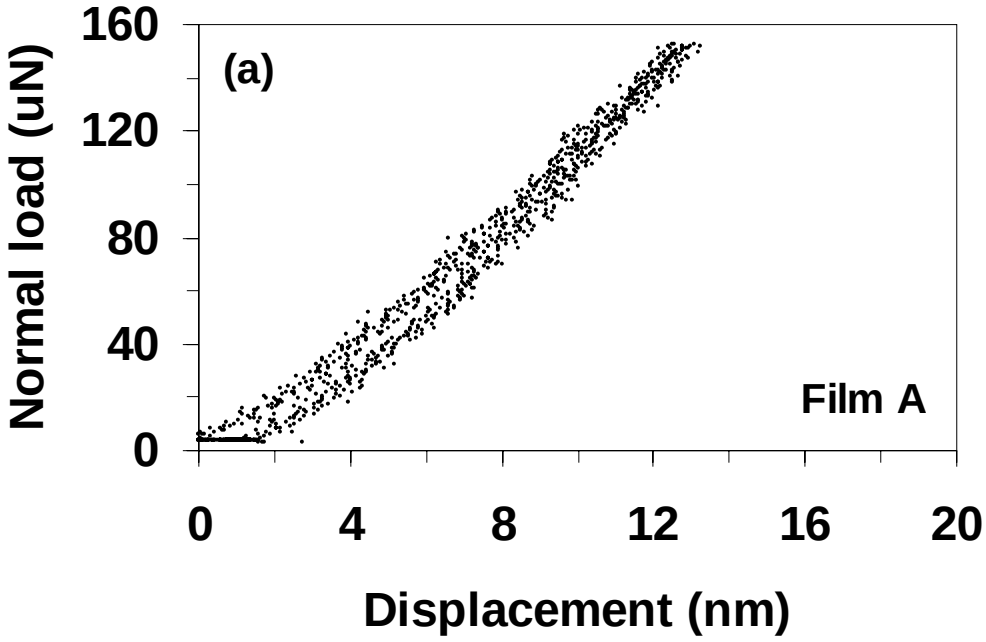
(a)
Film A
Normal load (uN)
Displacement (nm)
0
40
80
120
160
0
4
8
12
16
20

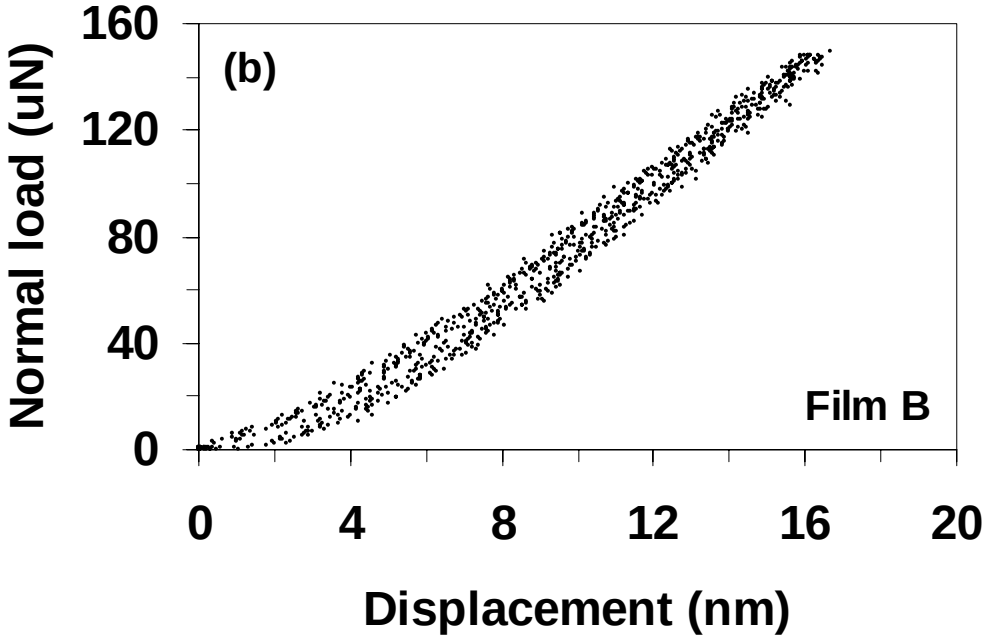
(b)
Film B
Normal load (uN)
Displacement (nm)
0
40
80
120
160
0
4
8
12
16
20

Figure 8

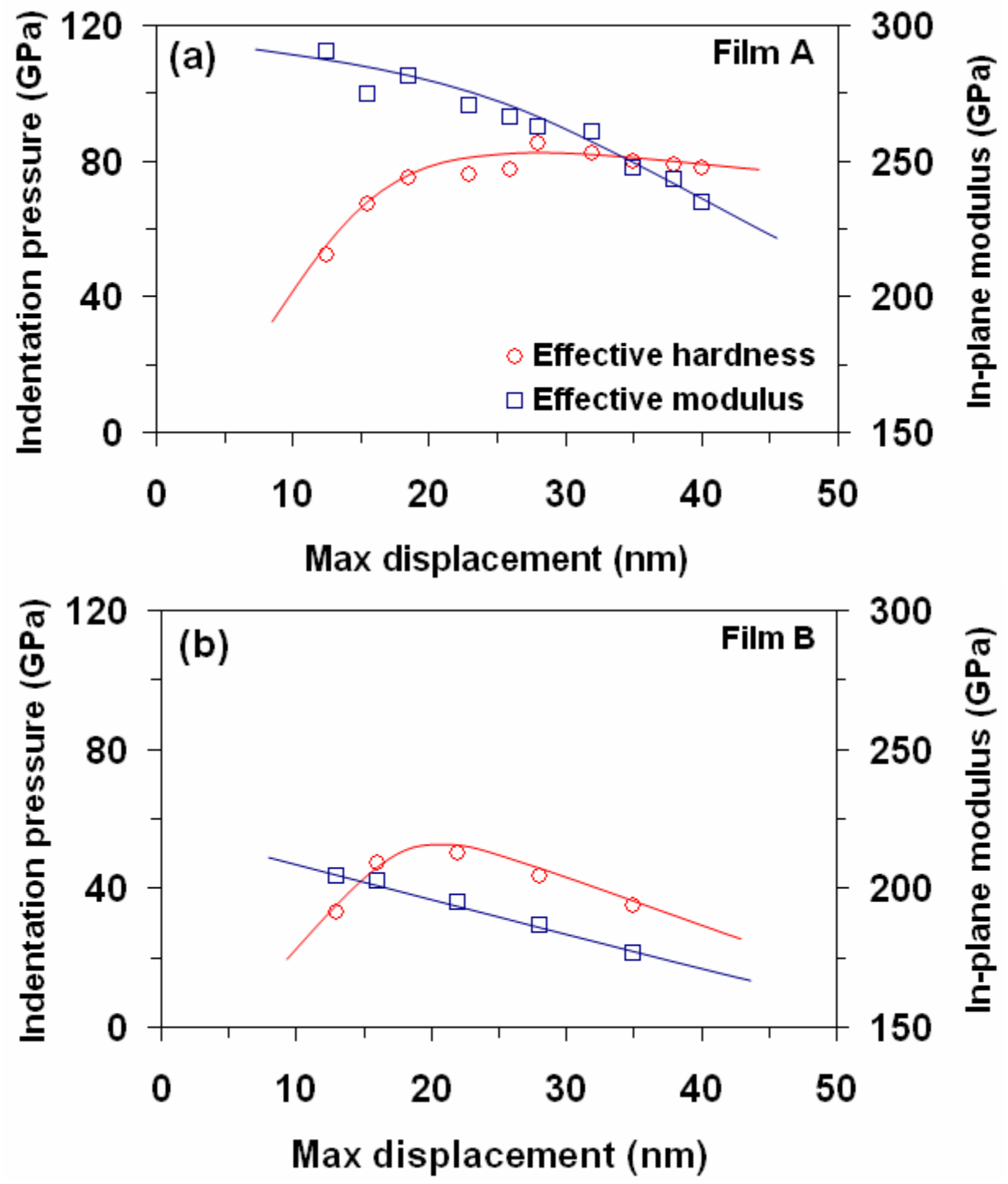
(a)
Film A
Effective hardness
Effective modulus
Indentation pressure (GPa)
In-plane modulus (GPa)
Max displacement (nm)
0
40
80
120
150
200
250
300
0
10
20
30
40
50
(b)
Film B
Indentation pressure (GPa)
In-plane modulus (GPa)
Max displacement (nm)

Figure 9